Active area optimisation of film bulk acoustic resonator for improving performance parameters

R. Patel✉, M.S. Adhikari and D. Boolchandani

In this Letter, an active area optimisation technique to improve the performance parameters of the film bulk acoustic resonator (FBAR) is proposed. The active area of the back trench membrane-based FBAR is optimised to remove the spurious modes, higher harmonic modes, and to confine the acoustic signal at its central part during the resonance. The effect of thickness variation of SiO_2 layer on the performance parameters was studied using finite-element analysis (FEA) simulation. The SiO_2 film, on silicon substrate, was used as the support layer and zinc oxide was used as the piezoelectric film for the resonator. The authors have successfully demonstrated the FBAR through FEA for an optimised active area of 320×320 μm^2, series resonance frequency (f_s) 1.249 GHz, and parallel resonance frequency (f_p) 1.273 GHz with an effective electromechanical coupling coefficient (k^2_{eff}) of 4.65%.

Introduction: In the film bulk acoustic resonator (FBAR) technologies, one of the major problems is the propagation of lateral (Lamb) wave, which cause the generation of unwanted spurious (transverse) modes and higher harmonic modes. In actual FBAR devices, owing to the discontinuous edges and boundaries, these excited spurious modes are able to induce new lateral modes. These transverse modes cause aggravating and unwanted ripples in the pass band of the filter and they also can diminish the quality factor because of energy conversion to these spurious modes [1–3].

Different solutions have been reported to remove or minimise the presence of spurious modes and higher harmonic modes using finite-element analysis (FEA) simulation, which includes apodisation technique, placement of Bragg reflection in periodic grating and addition of a thickened edge load on the top electrodes. In the apodisation (use of non-Manhattan geometries) technique, change in top electrode geometry such as pentagonal, trapezoidal, and hexagonal is required. This does not increase complications in the fabrication process of the resonator. Apodisation technique extends the path length of Lamb waves, and their resonance peaks were smeared out. However, with this technique the *Q*-factor obtained was not optimal, because spurious modes were minimised, but not completely eliminated [4, 5].

The placement of Bragg reflector in periodic grating results in the generation of the stop band. It plays a major role in suppressing the transverse resonances. Liu *et al.* [6] reported that a transverse-free fundamental resonance is obtained provided that period of grating and thickness is set so that the stop band covers the range of frequencies where the transverse mode resonances occur. This technique is effective to suppress the transverse resonances and improve the quality factor at the cost of reducing the effective electromechanical coupling coefficient [7].

Another method of addition of a thickened edge load on the top electrodes provides a more robust solution and achieves good values of *Q*-factor, as the lateral waves do not propagate through the structure. However, it increases complications in the fabrication process of the resonator and causes degradation in the electrical behaviour of the FBAR [8, 9].

There is no single technique available in the literature to suppress the spurious modes and higher harmonic modes together. These works propose an active area optimisation technique, which suppresses the spurious modes and higher harmonic modes with the confinement of the acoustic signal at its central part during the resonance. This technique does not increase complications in the fabrication process of the resonator.

Device structure and simulation: FBAR with a proposed operating frequency of 1.25 GHz was designed using zinc oxide (ZnO; 980 nm) as the piezoelectric (PZE) material and gold (Au) as the bottom and top electrodes (150 nm). The active area of the three designed FBARs was taken to be 225×225, 260×260, and 320×320 μm^2. All the layers in the 3D schematic of the FBAR and its 3D cross-sectional view are illustrated in Figs. 1 and 2, respectively. In Fig. 1, GSG represents the ground-signal-ground line for both of the input and output ports. The TE and BE represent the top and bottom electrodes of the resonator, respectively. The active area is shown in the centre of the resonator (in blue). The PZE layer lies between the BE and TE (in white).

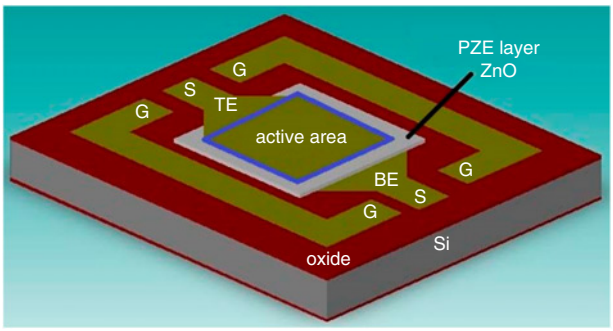

Fig. 1 *3D schematic of back trench membrane-based FBAR*

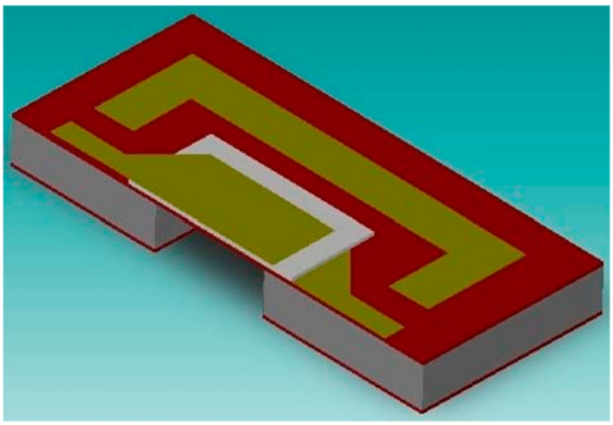

Fig. 2 *3D cross-sectional views of back trench membrane-based FBAR*

The 3D structure of the FBAR device was built, after the fabrication flow was specified in the process editor, material properties were defined in the material property database and 2D mask patterns were drawn using the layout editor. This 3D structure was meshed for FEA and analysed using the analyser module. The interaction between the electrical field and the displacement in the resonator was analysed, by FEA tool, using the following PZE constitutive equations [4]:

$$T_i = c^E_{ij} S_j - e_{ij} E_j \quad (1)$$

$$D_i = \varepsilon^S_{ij} E_j + e_{ij} S_j \quad (2)$$

where T_i, D_i, S_j, E_j, and e_{ij} are the stress, electric displacement, strain, electric field & PZE stress components, and c_{ij} & ε_{ij} are the stiffness & permittivity constants, respectively. The superscripts E and S denote that the corresponding constants, measured at a constant electric field and constant strain, respectively.

The hexagonal wurtzite structure along the *c*-axis of the ZnO film was used for the FEA simulation. The FBAR was simulated for DC, modal and harmonic analysis. The DC analysis of the FBAR was done using a Mem-Mech solver with a 1 V DC potential applied to the top Au electrode. This analysis was done to compute various important parameters such as the displacement of the PZE layer, the charge generated, and the static capacitance between both the electrodes. A modal analysis is then performed to estimate the frequency of the series and parallel breathing modes. These modes occur when the top and bottom surfaces of the PZE layer move longitudinally in opposite directions. The series resonance frequency, f_s, was obtained with closed circuit conditions, when both the electrodes are grounded. To compute the parallel resonance frequency, f_p, the modal analysis of the structure was obtained with an open circuit condition, when the bottom electrode was grounded and the top electrode was left floating. The method of excitation was longitudinal that resulted in the generation of the longitudinal mode, i.e. the thickness-extensional mode (TE), since *c*-axis ZnO was used for the PZE layer. The shear mode gets generated in two cases; by lateral excitation, in which we align both the electrodes parallel to the PZE film surface or by depositing the *c*-axis tilted ZnO

film as a PZE layer, both of these are not the case here [10]. In addition to the modal analysis, the harmonic analysis was done to obtain the impedance characteristic and the quality factor (Q) of FBAR.

Results and discussion: A novel concept of active area optimisation of FBAR has been described in this section to remove the spurious modes, higher harmonic modes, and to confine the acoustic signal at its central part during the resonance. The active area of FBAR should be chosen to cover the stop band only for the frequency range where the lateral modes and higher harmonic modes occur. A parametric sweep based study is used to analyse the effect of the active area on the performance characteristics. In this study, 3D FEA simulation was done for different active areas of which three cases have been discussed here for performance analysis. The active areas of these three cases have been selected as 225 × 225, 260 × 260, and 320 × 320 μm^2. In the DC analysis of the three FBARs, it was observed that the maximum 2 nm displacement, in the z-direction, for a DC voltage of 1 V is obtained for the case of FBAR with an active area of 320 × 320 μm^2. The PZE layer displacement generated a static charge between its top and bottom surfaces, resulting in a stack capacitance of 5 pF.

The spurious modes are generated either before the series resonant frequency or between the series and parallel resonant frequencies. However, the higher harmonic modes are generated after the parallel resonant frequency [11, 12]. The differences of fundamental, spurious, and higher harmonic modes are also illustrated by their mode shapes. Fig. 3 shows the breathing modes at the series resonance. Fig. 4 shows the case when a spurious mode gets generated whereas, Figs. 5 and 6 show the same when higher harmonic modes are generated. The mode shape of the second peak in Fig. 7 for the two cases of 225 × 225 and 260 × 260 μm^2 are shown in Figs. 5 and 6, respectively.

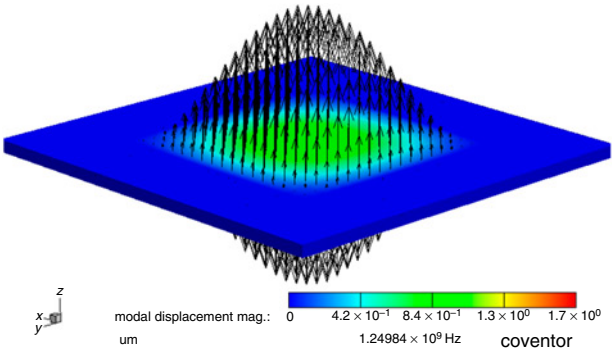

Fig. 3 *Breathing modes of series resonance*

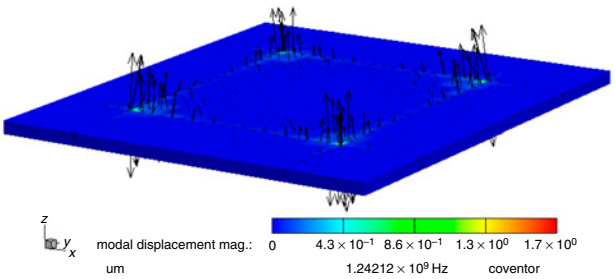

Fig. 4 *Breathing modes of spurious mode*

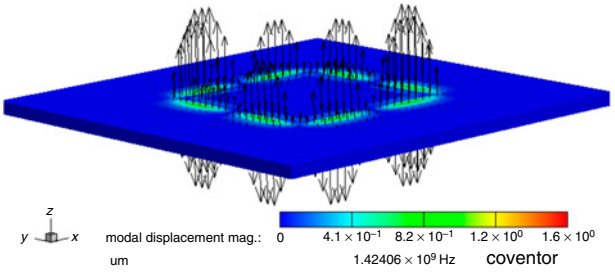

Fig. 5 *Breathing modes of higher harmonic mode of active area 225 × 225 μm^2*

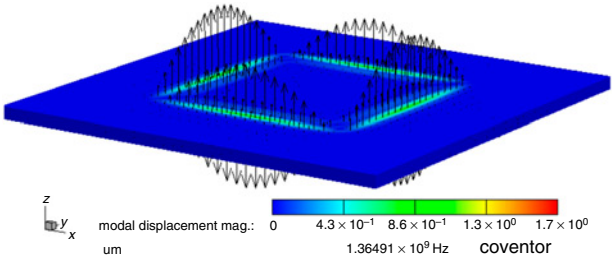

Fig. 6 *Breathing modes of higher harmonic mode of active area 260 × 260 μm^2*

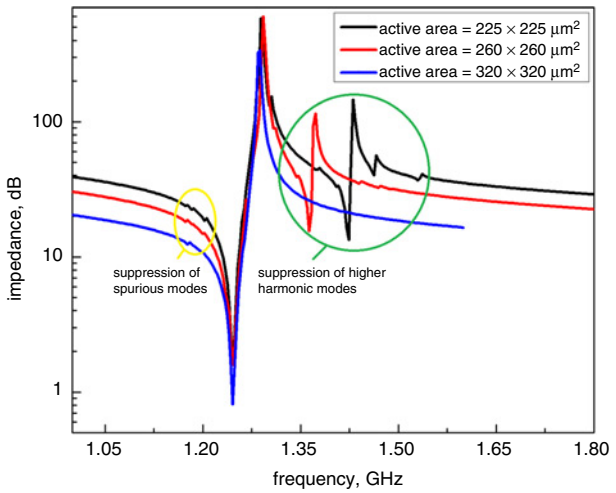

Fig. 7 *Impedance characteristic as function of frequency for different active area*

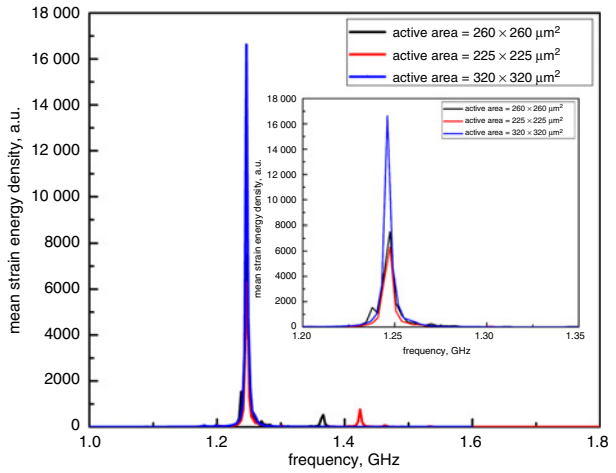

Fig. 8 *Mean strain energy density distribution with frequency*

The impedance characteristic as a function of frequency is depicted in Fig. 7. Series of spurious modes and higher harmonic modes were seen above the parallel resonance frequency f_p occurring due to the lateral propagation of the eigen Lamb waves. It is clear from the impedance characteristics that both the spurious and higher harmonic modes that are generated for the cases with active areas of 225 × 225 and 260 × 260 μm^2 disappear for the case of FBAR with an active area of 320 × 320 μm^2. As the active area was greater than the cavity area, a stop band was induced which plays an important role in suppressing the spurious transverse resonances. It results in better confinement of acoustic signals at the central part of the FBAR with an active area of 320 × 320 μm^2 that also provides the maximum displacement in the longitudinal direction and minimum displacement in the lateral direction. Fig. 8 shows the higher energy confinement for an active area of 320 × 320 μm^2 as compared to the two other active areas (225 × 225 and 260 × 260 μm^2). The mean strain energy density distribution with a frequency clearly indicates that all the energy is confined at fundamental mode for the active area of 320 × 320 μm^2, while in other

two active areas (225 × 225 and 260 × 260 μm^2), it gets distributed to the higher harmonic modes.

Effect of SiO_2 layer thickness on the performance characteristics: A parametric sweep-based study has been used to understand the effect of oxide (SiO_2) layer thickness on the performance characteristics of the FBAR. The thickness of the oxide layer was varied from 446 to 896 nm with a step size of 150 nm. The impedance characteristic as a function of frequency is shown in Fig. 9 and it is observed that the resonant frequency decreases with the increasing oxide thickness.

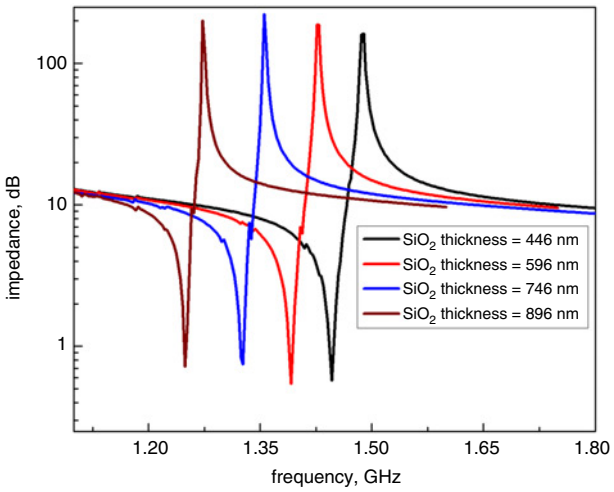

Fig. 9 *Impedance characteristic as function of frequency for different SiO_2 thickness*

This was due to the mass loading of the SiO_2 layer. The electromechanical coupling coefficient of the resonator is improved with the decreasing thickness of the oxide layer because of better confinement of acoustic signal. More vibration energy of thin film can permeate into the SiO_2 layer, but due to the high acoustic impedance ratio between the PZE and SiO_2 layers, complete reflection of the acoustic signal takes place. This results in the reduction of loss of energy in the SiO_2 layer. One another reason of increase in the Q factor is that the SiO_2 is a low loss material.

The value of quality factor (Q) is increased with the increasing thickness of oxide layer. The coupling coefficient k^2_{eff} of the resonator varies approximately as $1/t$, where t is the thickness of the composite active area of the resonator. This is the logical tendency, as the electric field within ZnO and its volume fraction are diminishing with increasing t. Simulated results confirmed that the performance parameters series resonant frequency (f_s), parallel resonant frequency (f_p), quality factors (Q_s & Q_p) and the effective electromechanical coupling coefficient (k^2_{eff}) strongly depends on the thickness of the deposited SiO_2 layer. It is observed that there is a trade-off between the quality factor and the effective electromechanical coupling coefficient [13]. An increase in SiO_2 thickness results in corresponding increase in the quality factor and decrease in k^2_{eff}. The variations of performance parameters with oxide thickness are shown in Table 1.

Table 1: Variations of performance parameters with oxide thickness

SiO_2 thickness, nm	f_s, GHz	f_p, GHz	k^2_{eff}, %	Q_s	Q_p
446	1.446	1.489	7.06	428.8	426
596	1.391	1.426	6.07	482	479.7
746	1.327	1.355	5.17	585	630
986	1.249	1.273	4.65	726	763.5

Conclusion: In this work, the concept of active area optimisation is proposed, using FEA simulations, to remove the spurious modes, higher harmonic modes and to confine the acoustic signal at its central part during the resonance. A parametric sweep-based FEA is used to understand the effect of SiO_2 layer thickness on the performance characteristics of the FBAR. Simulated results confirmed that the performance parameters f_s, f_p, Q_s, Q_p, and k^2_{eff} strongly depend on the thickness of the deposited SiO_2 layer. The proposed optimised device with the active area (320 × 320 μm^2) had quality factors, Q_s, of 726 and, Q_p, of 763.5 with corresponding figure of merits of 33.76 and 35.50, respectively.

Acknowledgments: The author would like to acknowledge the support of the TEQIP-III (A Government of India Project assisted by the World Bank), for providing a research grant under TEQIP Collaborative Research Scheme (grant no. 1-5744664011).

Submitted: *05 July 2020* E-first: *14 September 2020*
doi: 10.1049/el.2020.1901
One or more of the Figures in this Letter are available in colour online.

R. Patel (*MBM Engineering College, Jodhpur, Rajasthan, India*)

✉ E-mail: teqip.raju.ece@jnvu.edu.in

M.S. Adhikari (*Lovely Professional University, Phagwara, Punjab, India*)

D. Boolchandani (*Malaviya National Institute of Technology, Jaipur, Rajasthan, India*)

References

1 Pensala, T., and Ylilammi, M.: 'Spurious resonance suppression in gigahertz-range ZnO thin-film bulk acoustic wave resonators by the boundary frame method: modeling and experiment', *IEEE Trans. Ultrason. Ferroelectr. Freq. Control*, 2009, **56**, (8), pp. 1731–1744
2 Chen, D., Wang, J.J., Xu, Y., *et al.*: 'Film bulk acoustic biosensor for detection of trace pesticide residues in agricultural products', *Electron. Lett.*, 2013, **49**, (15), pp. 924–925
3 Chen, D., and Wang, J.J.: 'Lateral field excited film bulk acoustic resonator for detection of protein–ligand interactions', *Electron. Lett.*, 2012, **48**, (19), pp. 1178–1179
4 Pillai, G., Zope, A.A., Tsai, J.M.L., *et al.*: 'Design and optimization of SHF composite FBAR resonators', *IEEE Trans. Ultrason. Ferroelectr. Freq. Control*, 2017, **64**, (12), pp. 1864–1873
5 Yang, D.Y., and Kim, H.W.: 'Film bulk acoustic resonator with improved lateral mode suppression', U.S. Patent 6,693,500, 2004
6 Liu, J., Omori, T., Ahn, C., *et al.*: 'Impact of surface periodic grating on film bulk acoustic resonator structures to spurious transverse resonances', *J. Appl. Phys.*, 2013, **113**, (14), p. 144507
7 Serhane, R., Hadj-Larbi, F., Hassein-Bey, A., *et al.*: 'Selective band gap to suppress the spurious acoustic mode in film bulk acoustic resonator structures', *J. Vib. Acoust.*, 2018, **140**, (3), p. 031018
8 Thalhammer, R., Kaitila, J., Zieglmeier, S., *et al.*: '4E-3 spurious mode suppression in BAW resonators'. IEEE Ultrasonics Symp., Vancouver, BC, Canada, 2006, pp. 456–459
9 Yakimenko, Y., Zazerin, A., Orlov, A., *et al.*: 'Film bulk acoustic resonator finite element model in active filter design'. IEEE Proc. 37th Int. Spring Seminar on Electronics Technology, Dresden, Germany, 2014, pp. 486–490
10 Chen, D., Ren, W., Song, S., *et al.*: 'The high Q factor lateral field-excited thickness shear mode film bulk acoustic resonator working in liquid', *IEEE Micromach.*, 2016, **7**, (12), p. 231
11 Kaitila, J., Ylilammi, M., Ella, J., *et al.*: 'Spurious resonance free bulk acoustic wave resonators'. IEEE Symp. on Ultrasonics, 2003, vol. 1, pp. 84–87
12 Kaitila, J.: '3C-1 review of wave propagation in BAW thin film devices-progress and prospects'. IEEE Symp. on Ultrasonics Proc., 2007, pp. 120–129
13 Artieda, A., and Muralt, P.: 'High-Q AlN/SiO_2 symmetric composite thin film bulk acoustic wave resonators', *IEEE Trans. Ultrason. Ferroelectr. Freq. Control*, 2008, **55**, (11), pp. 2463–2468